Asian Journal of Chemistry; Vol. 38, No. 3 (2026), 774-780
ASIAN JOURNAL OF CHEMISTRY
https://doi.org/10.14233/ajchem.2026.35347

Design and Fabrication of $CsSnI_3$ Electrodes with 2D Perovskite (BA_2SnI_4)-Enhanced PVDF-HFP Gel Polymer Electrolytes for Advanced Solid-State Supercapacitor Devices

NIDHI YADAV[1], NAVNEET KUMAR[1,*] and MRINMOY KUMAR CHINI[2]

[1]Department of Chemistry, Faculty of Engineering, Teerthanker Mahaveer University, Moradabad-244001, India
[2]Department of Applied Sciences (Chemistry), Galgotias College of Engineering & Technology, Greater Noida-201306, India

*Corresponding author: E-mail: navkchem@gmail.com; drnavneet.engineering@tmu.ac.in

Received: 28 November 2025 *Accepted*: 3 February 2026 *Published online*: 6 March 2026 AJC-22297

In this study, a novel symmetric solid-state supercapacitor was fabricated by integrating lead-free $CsSnI_3$ perovskite electrodes with a 2D Ruddlesden-Popper (BA_2SnI_4)-reinforced PVDF-HFP/$NaPF_6$ gel polymer electrolytes (GPEs). Composite GPEs were prepared *via* a solution-casting method with varying BA_2SnI_4 contents (0-20 wt.%) to enhance ionic conductivity, mechanical flexibility, and interfacial stability. Among the prepared samples, the optimized PNPS3 electrolyte containing 15 wt.% BA_2SnI_4 exhibited the highest ionic conductivity of 1.12 mS cm^{-1} and lowest bulk resistance (92 Ω), attributed to the formation of efficient ion-hopping pathways and reduced polymer crystallinity. The structural analyses confirmed the successful incorporation of layered BA_2SnI_4 nanosheets and the formation of highly crystalline orthorhombic black-phase $CsSnI_3$ electrodes. With an energy density of 25.8 Wh kg^{-1}, a power density of around 500 Wh g^{-1}, a low IR drop (0.042 V), an equivalent series resistance of 4.8 Ω and a charge transfer resistance of 12.6 Ω, an optimized symmetric $CsSnI_3$/PNPS3/$CsSnI_3$ devices produced a high specific capacitance at 186 F g^{-1} at 1 A g^{-1}. After 5000 cycles, the device showed outstanding cycling stability, maintaining 92% with its initial capacitance with a coulombic efficiency of >97%. The composite electrolyte membrane sustained over 1000 bending cycles, confirming its mechanical robustness for flexible applications. The enhanced electrochemical performance is attributed to the synergistic coupling between conductive $CsSnI_3$ electrodes and the layered BA_2SnI_4-reinforced polymer matrix, which promotes rapid Na^+ transport, stable interfaces and suppressed degradation. For next-generation energy storage devices, this work offers an efficient method for developing flexible, high-energy-density and eco-friendly solid-state supercapacitors.

Keywords: $CsSnI_3$ electrode, BA_2SnI_4, PVDF-HFP, Gel polymer electrolyte, Solid-state supercapacitor.

INTRODUCTION

Recent progress in research has shown that perovskite materials have the ability of allowing defect tolerance, carrier dynamics and electrochemical activity that are second to none and has further demonstrated that the material can be used in the configuration of supercapacitor; through the materials exhibiting more advanced [1-3]. The perovskites, with lead-free tin-based halide perovskites, especially $CsSnI_3$, is having become the green alternatives to Pb-based perovskites in the family [4,5]. $CsSnI_3$ shows high electrical conductivity, charge transport by defect and good band alignment qualities which are necessary in high performance electronic materials. $CsSnI_3$ is, however, reported to be prone to oxidation (Sn^{2+} to Sn^{4+}), which means that measures should be taken to stabilize the perovskite crystal structure and inhibit the degradation routes [6]. Previous experiments indicate that the orthorhombic black phase can be strengthened through structural design and ionic modification, enhancing thermal and environmental stability [7,8]. More knowledge of the phase transitions and the oxidation processes has advanced the insight into the behaviour of $CsSnI_3$ under an electrochemical condition, further highlighting the importance of chemical reinforcement by the use of such interfaces [9]. These theoretical studies are complemented by complementary theoretical studies which have demonstrated that it has high carrier mobility and could be useful in photovoltaics and thermophotovoltaic equipment, enhancing its potential in other electronic and electrochemical applications [10]. Such results demonstrate that $CsSnI_3$ is an attractive solid-state electrode material in supercapacitors, especially in combination with a high-performing electrolyte.

Simultaneously with the work on electrode development, much has been done on two-dimensional (2D) Ruddlesden-Popper perovskites, *e.g.* BA_2SnI_4, in order to enhance ionic mobility and interfacial properties in polymer matrices [11]. Their ion-hopping channels are generated in a somewhat interrelatable geometry, which increases their dielectric properties and ionic conductivity. Recent studies show that BA_2SnI_4 has a high excitonic behaviour, stable nanostructuring and controlled crystallinity, hence can be used as a hybrid composite systems [12]. Tuning in BA_2SnI_4 using chloride has demonstrated better film morphology, defect elimination and charge transportation and this has verified that these materials can be chemically manipulated to respond to the chemical changes [13]. Other research reports include its capacity to produce pinhole-free crystalline layers and uniform thin films, which are part of the stable, compact and efficient ion transport routes [14]. Multifunctional optical and structural characteristics of 2D hybrid perovskites also facilitate their usage in polymer matrices meant to be used in flexible electrochemical devices [15].

PVDF-HFP-based gel polymer electrolytes have also proven to be important building blocks in solid-state devices because of their wide electrochemical stability window, mechanical flexibility and semi-crystalline structure that easy ion movement [16]. Their porous structure and high dielectric constant make them to dissociate ionic salts including $NaPF_6$ and increase ionic conductivity [17]. Lithium-ion and sodium-ion systems with thermally stable and robust GPEs that are based on PVDF-HFP have been reported, which show excellent mechanical and electrochemical performance [18]. Later advances which have involved ionic liquids and sodium salts have allowed more flexibility and thermal performance to the supercapacitor devices [19]. Further on, the addition of ethylene carbonate and propylene carbonate as plasticizers contributes greatly to segmental movements and conductivity in $NaPF_6$-based PVDF-HFP films as evidenced in sodium-ion polymer electrolyte researches [20]. It is also demonstrated that the electrochemical behaviour of PVDF-HFP matrices is modulated by the ion-solvation environment of the ionic liquids with different anions, which are introduced into the matrices [21]. Taken together, these results make PVDF-HFP/$NaPF_6$ systems attractive candidates in the development of solid-state supercapacitors based on GPE.

Recent comparative analysis of GPE-based supercapacitors highlights the importance of optimisation of ion-transport pathways, mechanical stability and interfacial charge transfer in order to maximise performance [22]. There have been a series of works incorporating safe solvents, interpenetrating polymer arrays or other polymer phases in high-performance PVDF-HFP electrolytes to increase ionic conductivity and mechanical stability [23-25] and PAN/PVDF-HFP systems have demonstrated much-improved ionic conductivity and thermal stability in gel electrolyte systems [26,27]. Also, SN-modified PVDF-HFP electrolyte have demonstrated better ion conduction and stable electrochemical cycling [28]. Adjunctive advances in polymerised ionic liquid GPEs highlight the fact that they can retain their electrochemical stability despite repeated cycling [29]. Extensive review studies affirm that future generation high-performance solid-state supercapacitors depend on advanced GPE design to provide functionality to these devices [30].

In spite of these developments, the integrated combination of $CsSnI_3$ electrodes with BA_2SnI_4 improved PVDF-HFP GPEs is not extensively studied especially in case of symmetric solid-state supercapacitors. The present work effectively addresses gap by synthesizing a 2D perovskite-reinforced GPE system and combining it with electrodes made of $CsSnI_3$ in order to take advantage of synergies in ionic conductivity, mechanical flexibility, structural stability and electrochemical performance. This combined strategy is offering an effective pathway to the creation of high-performance, flexible and safe solid-state energy storage.

EXPERIMENTAL

Polyvinylidene fluoride-*co*-hexafluoropropylene (PVDF-HFP) was used as the host polymer due to its semi-crystalline nature, electrochemical stability and mechanical strength, sodium hexafluorophosphate ($NaPF_6$) was incorporated to supply Na^+ charge carriers within the polymer matrix. Plasticizers were added to the polymer electrolyte system by adding ethylene carbonate (EC) and propylene carbonate (PC in mass ratio 1:1) to improve the mobility of segments and the amorphous content of the system. The functional nano-additive was the 2D-layered perovskite BA_2SnI_4 (butylammonium tin iodide) to be incorporated into the polymer film to increase ionic conductivity and interfacial stability. N,N-Dimethylformamide (DMF) was used as solvent for casting as it has great solubility with PVDF-HFP and perovskite material. In the development of electrodes, cesium iodide (CsI) and tin(II) iodide (SnI_2) were taken as a precursor to prepare $CsSnI_3$ that acted as active electrode material. All the moisture-sensitive perovskite materials were manipulated in a nitrogen glovebox to prevent degradation and conductive current collectors or ITO substrates were employed to assemble a final device.

Synthesis of 2D perovskite integrated gel polymer electrolytes (GPEs): Solution-casting process was used to synthesize the gel polymer electrolytes. Briefly, 1.0 g of PVDF-HFP was dissolved in DMF in a stirred with constant temperature maintained at 60 °C until a clear polymer solution was formed. This solution was then stirred with 1.0 g of $NaPF_6$ until the entire amount of salt dissociated. The mixture of plasticizers (1.0 g of EC and PC 1:1 ratio) was added further to decrease crystallinity and provide increased flexibility and ionic mobility of the polymer. Then, BA_2SnI_4 (0-20 wt.%) was added in minimum amount of DMF under ultrasonic stirring (10-15 min) to disperse the agglomerates and achieve uniform dispersion of nanosheets. Finally, it was gently mixed with the polymer-salt-plasticizer solution and stirred in a sufficiently slow manner so as to obtain entire homogenize nanosheet dispersion.

This electrolyte solution was slowly evaporated at room temperature on a clean glass plate to retrieve thin and clear and flexible GPE films. The films were carefully removed and placed in a dry box to ensure complete drying before characterisation. The four ready-made compositions were named PNPS1 to PNPS4 and are listed in Table-1.

Electrode preparation and device fabrication

Preparation of $CsSnI_3$ electrode: The $CsSnI_3$ electrodes were prepared by solution based on the deposition process. A

TABLE-1
COMPOSITION OF PVDF-HFP BASED
GPEs WITH VARYING BA_2SnI_4 CONTENT

Sample ID	PVDF-HFP (g)	$NaPF_6$ (g)	EC:PC (g)	BA_2SnI_4 (wt.%)
PNPS1	1.0	1.0	1.0	0
PNPS2	1.0	1.0	1.0	10
PNPS3	1.0	1.0	1.0	15
PNPS4	1.0	1.0	1.0	20

precursor solution was perpared by adding stoichiometric quantities of CsI and SnI_2 in DMF:DMSO solution mixture (4:1 ratio) while stirring at 70 ºC until a dark-red solution had been obtained. At the same time, acetone, isopropyl alcohol and deionised water were used to test clean the current collector substrates sequentially through ultrasonication and then dried in warm air. $CsSnI_3$ precursor solution was then spin-coated or doctor-bladed and uniformly spread on the substrates. The coated films were annealed at 120-150 ºC in a nitrogen atmosphere for 20-30 min to induce crystallization of black-phase $CsSnI_3$. The obtained electrodes were uniform on the surface, sufficiently thick and highly electrically conductive, which qualifies them as an electrode to be used in symmetric supercapacitor-based devices.

Device fabrication (sandwich supercapacitor): The solid-state symmetric supercapacitor was configured as a sandwich structure of current collector/$CsSnI_3$ active electrode/ PVDF-HFP + BA_2SnI_4 GPE/$CsSnI_3$ active electrode/current collector. For assembly, the optimised GPE films were cut to the required size and carefully placed between two identical $CsSnI_3$ coated electrodes. Gentle pressure was applied to ensure good contact and minimize interfacial resistance. The encapsulation was then performed using a polymer sealing layer or epoxy resin to protect the perovskite-based elements from moisture and other environmental factors. The constructed devices were allowed to stabilize under ambient conditions in 12 h to enable interface stabilisation before subjecting the devices to structural and electrochemical characterisation.

RESULTS AND DISCUSSION

Ionic conductivity: The electrochemical impedance spectroscopy (EIS) was employed to assess the ionic conductivity of the prepared gel polymer electrolytes (GPEs). In the Nyquist plots (Fig. 1), the high-frequency semi-circle corresponds to bulk resistance, whereas the low-frequency linear patterns reflect the capacitive behaviour. Upon incorporation of BA_2SnI_4 nanosheets, a clear improvement in the ionic conductivity was observed. The progressive decrease in semi-circle diameter from PNPS1 to PNPS4 indicates a reduction in bulk resistance. As summarized in Table-2, the pristine polymer (PNPS1) exhibited the lowest conductivity due to restricted ion mobility, while PNPS3 showed the highest conductivity, attributed to the optimal formation of interconnected ion-transport channels. A slight decrease in the conductivity for PNPS4 (filler content >15 wt.%) is likely due to nanosheet agglomeration, which obstructs continuous ion pathways.

Mechanical flexibility: The mechanical flexibility tests indicated that all GPE films were flexible to bending but the

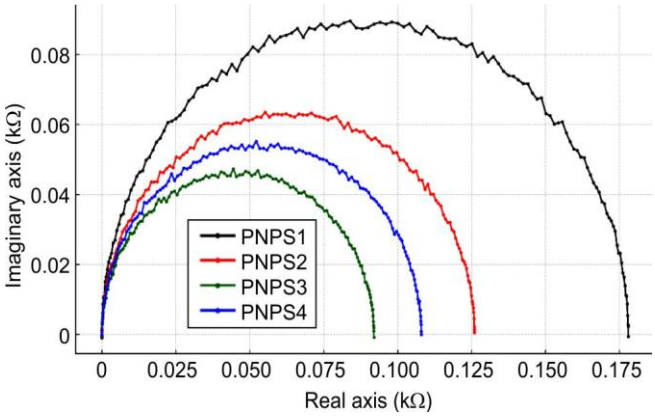

Fig. 1. Nyquist plots of GPE samples PNPS1-PNPS4

TABLE-2
IONIC CONDUCTIVITY VALUES OF
GPE SAMPLES AT ROOM TEMPERATURE

Sample ID	Bulk resistance (Ω)	Ionic conductivity (mS/cm)
PNPS1	178	0.48
PNPS2	126	0.69
PNPS3	92	1.12
PNPS4	108	0.91

presence of BA_2SnI_4 had significant impacts on the elasticity of the film. As shown in Fig. 2, sample PNPS1 exhibited moderate flexibility but inclined to form microcracks at high bending angles due to insufficient plasticization. In contrast, PNPS2 and PNPS3 maintained structural integrity and showed no visible damage even when bent to 180º. The addition of excessive amounts of filler (PNPS4) led to the partial brittleness resulting in reduced polymer chain mobility. According to Table-3, sample PNPS3 demonstrated the highest mechanical strength, remaining intact after 1000 bending cycles.

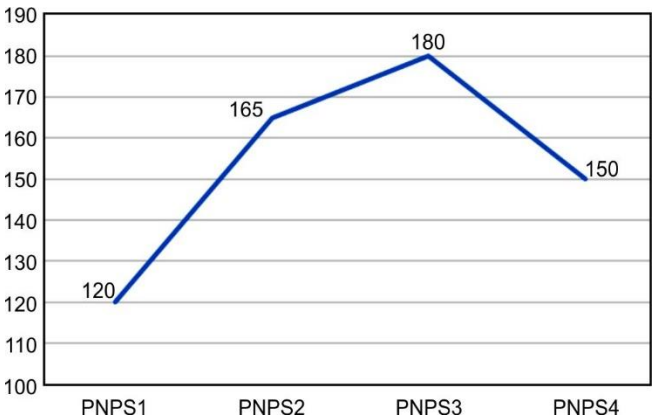

Fig. 2. Bending flexibility test images of GPE films at various angles

TABLE-3
MECHANICAL FLEXIBILITY AND
BENDING ENDURANCE OF GPEs

Sample ID	Maximum bending angle (º)	Bending cycles before failure
PNPS1	120	420
PNPS2	165	780
PNPS3	180	>1000
PNPS4	150	650

Thermogravimetric analysis (TGA): As shown in Fig. 3, all samples exhibited two-stage thermal degradation *i.e.* the first stage corresponds to the evaporation of residual solvent and plasticizer, while the second stage is associated with polymer chain decomposition. The addition of BA_2SnI_4 increased the decomposition temperature of the GPEs, as shown in Table-4. Among the samples, PNPS3 displayed the highest thermal stability, indicating that an optimal amount of perovskite enhances polymer–filler interactions and reduces thermal chain scission.

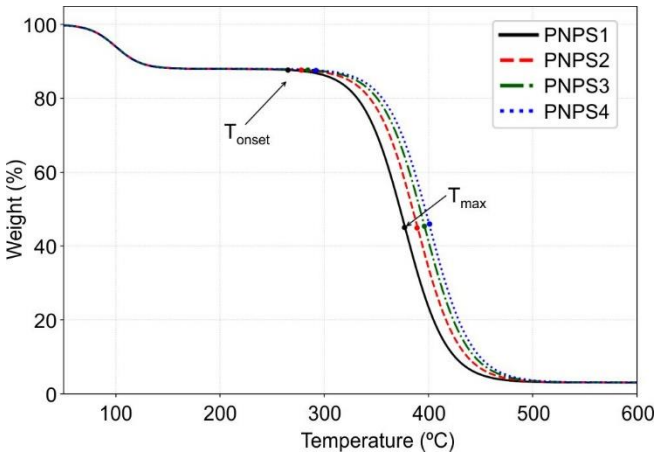

Fig. 3. TGA showing thermal decomposition of GPE samples

TABLE-4
TGA DECOMPOSITION TEMPERATURES OF GPE SAMPLES

Sample ID	Onset degradation (ºC)	Maximum degradation (ºC)
PNPS1	265	377
PNPS2	278	389
PNPS3	292	401
PNPS4	284	396

Structural and morphological analysis

XRD studies: Fig. 4 presents the XRD patterns of $CsSnI_3$ electrode and GPE samples. The presence of sharp orthorhombic $CsSnI_3$ peaks in the XRD pattern (Fig. 4a) demonstrates phase purity and proper crystallization during nitrogen annealed at 120-150 ºC. The diffraction peaks at 14º, 28º, 31º and 40º (2θ) were indexed to (100), (200), (210) and (220) planes, respectively, confirmed the clear crystal orientation and high crystallinity. Lack of secondary impurities such as Cs_2SnI_6 or unreacted SnI_2 further proved the presence of phase pure $CsSnI_3$. The sharp and intense peaks indicate uniform grain growth and high crystallinity, which enhance the electrical conductivity and charge transport.

The PVDF-HFP matrix had typical peaks of about 2θ ≈ 18º and 20º whereas the addition of BA_2SnI_4 formed other low angle reflections of 4-6º, which validated the layer structure (Fig. 4b). The peak intensity increased with higher perovskite loading, confirming successful incorporation of the material. Table-5 summarizes the crystallite size and its corresponding peak positions. The electrodes with $CsSnI_3$ exhibited different diffraction peaks, which are attributed to the black-phase orthorhombic structure, an indication of successful synthesis.

TABLE-5
XRD PEAK POSITIONS AND
CRYSTALLITE SIZES OF GPE SAMPLES

Sample ID	Major PVDF-HFP peak (2θ)	BA_2SnI_4 peak (2θ)	Crystallite size (nm)
PNPS1	18.1º, 20.2º	–	21
PNPS2	18.2º, 20.1º	4.8º	24
PNPS3	18.0º, 20.0º	4.7º	28
PNPS4	18.3º, 20.3º	4.6º	26

FESEM analysis: Fig. 5 displays the FESEM images representing the clear morphological differences among the GPE samples. Sample PNPS1 displayed a rough and non-uniform surface with visible micro-voids. After the addition of BA_2SnI_4 nanosheets, samples PNPS2 and PNPS3 exhibited a denser and more uniform structure, indicating improved matrix packing and better pathways for ion transport. In contrast, sample PNPS4 showed slight particle agglomeration due to excess filler content. The $CsSnI_3$ electrode surface appeared dense, fine-grained, and uniformly distributed, which supports efficient charge transport.

Electrochemical performance

Cyclic voltammetry (CV): Fig. 6 represents the CV curves of the symmetric supercapacitor devices. The device

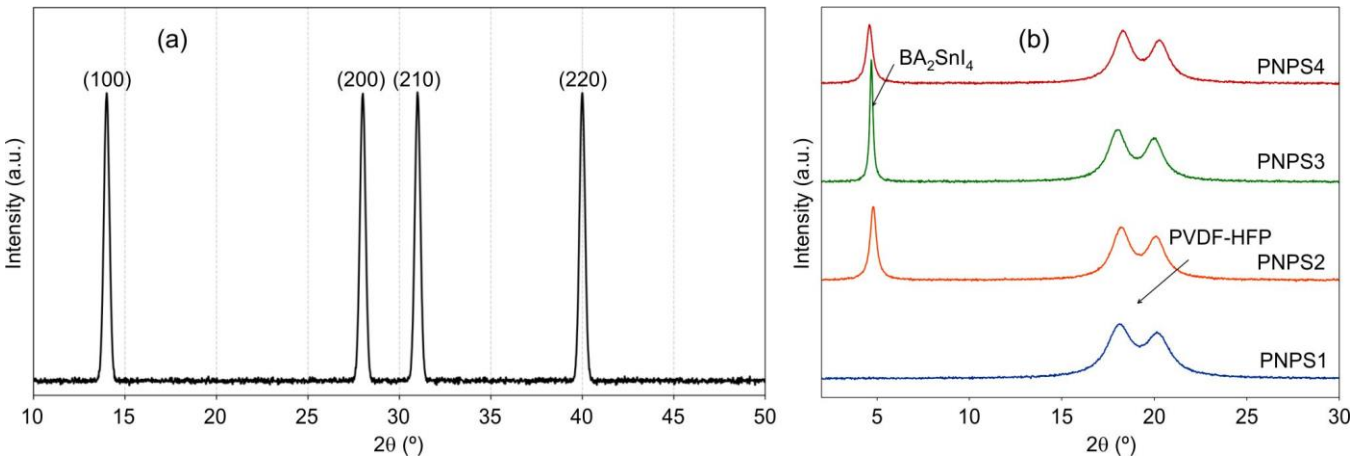

Fig. 4. XRD patterns of (a) $CsSnI_3$ electrodes and (b) PVDF-HFP GPEs

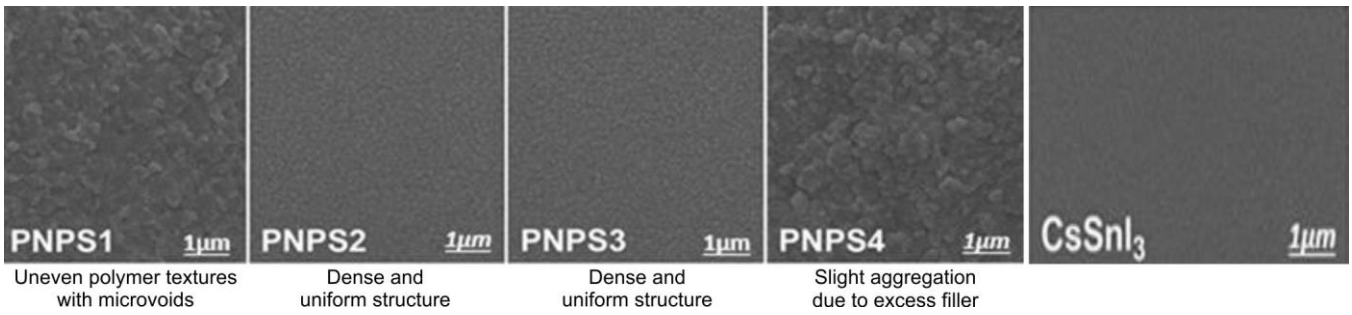

Fig. 5. FESEM micrographs showing surface morphology of GPEs and $CsSnI_3$ films

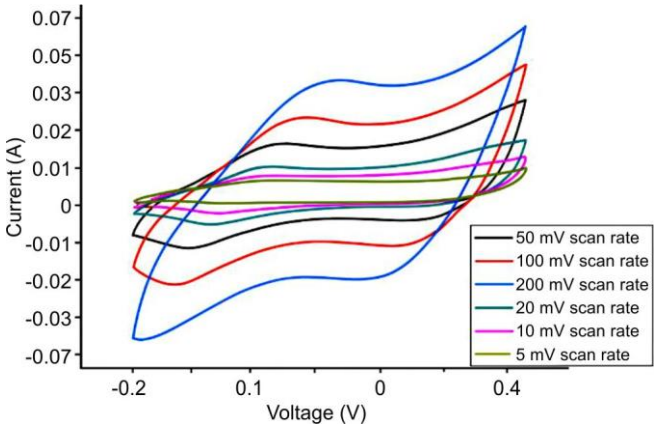

Fig. 6. Symmetric supercapacitor CV curves at various scan speeds

containing PNPS3 showed the largest enclosed area in the CV curves, indicating superior capacitive performance. Its nearly rectangular CV shape confirms ideal pseudocapacitive behaviour with minimal ohmic drop. The retention of this rectangular profile at higher scan rates suggests fast ion transport within the GPE matrix.

Galvanostatic charge-discharge (GCD): The GCD performance of the symmetric solid-state supercapacitor fabricated with the optimized PNPS3 (15 wt.% BA_2SnI_4) gel polymer electrolyte was evaluated at current densities from 0.5 to 5 A g^{-1} within a voltage window of 0-1.0 V. The GCD curves (Fig. 7) show nearly symmetrical triangular shapes with very low IR drop, indicating good reversibility, high coulombic efficiency, and excellent capacitive behaviour.

The linear and symmetric charge-discharge profiles confirm dominant pseudocapacitive behaviour and fast Na^+ ion transport across the $CsSnI_3$ electrodes, supported by the high conductivity of the PNPS3 matrix. The device carried a specific capacitance of 186 F g^{-1} at 1 A g^{-1}, with a low IR drop of 0.042 V and a coulombic efficiency of 98.4%.

The specific capacitance (C_S) was calculated using:

$$C_S = \frac{I\Delta t}{m\Delta V}$$

where I is the discharge current; Δt is the discharge time; m is the total mass of active material in both electrodes; and ΔV is the effective voltage excluding the IR drop.

The rate capability study showed capacitance values of 201, 186, 167, 152, and 131 F g^{-1} at 0.5, 1, 2, 3 and 5 A g^{-1}, respectively, with 65% capacitance retention at 5 g^{-1}. This good rate performance is attributed to the high ionic conductivity of PNPS3 (1.12 mS cm^{-1}), uniform dispersion of BA_2SnI_4 nanosheets and improved electrode-electrolyte contact. The low IR drop further confirms low internal resistance and enhanced ion diffusion due to the layered BA_2SnI_4 ion-transport pathways within the PVDF-HFP framework.

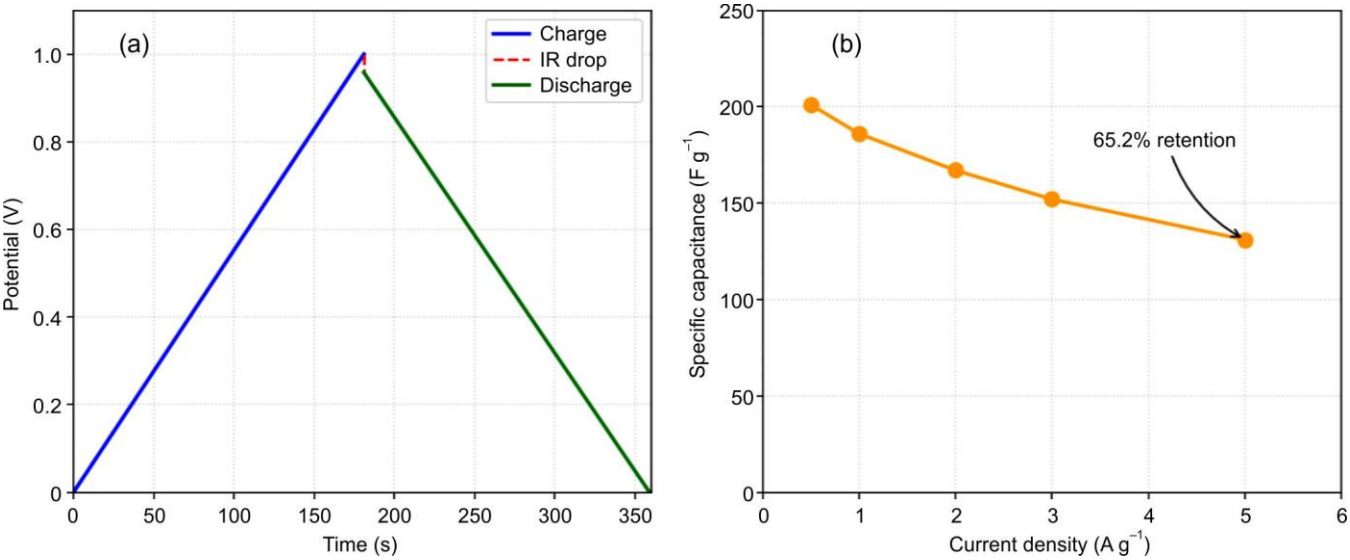

Fig. 7. (a) GCD profiles of the optimized PNPS3 (15 wt.% BA_2SnI_4) solid-state supercapacitor at 1 A g^{-1}, (b) Rate performance and capacitance retention at different current densities (0.5-5 A g^{-1})

The energy density (E) and power density (P) were calculated using the following eqns:

$$E = \frac{1}{2}\frac{C_S(\Delta V)^2}{3.6}$$

$$P = \frac{E \times 3600}{\Delta t}$$

The device achieved a high energy density of 25.8 Wh kg^{-1} and a power density of about 500 W kg^{-1}. These results indicate that the $CsSnI_3$/PNPS3-based symmetric solid-state supercapacitor shows balanced energy and power performance, making it suitable for flexible solid-state energy storage applications.

Electrochemical impedance spectroscopy (EIS): The internal resistance and interfacial charge-transfer behaviour of the symmetric solid-state supercapacitor were analyzed by EIS at open-circuit voltage over a frequency range of 100 kHz to 0.01 Hz. The Nyquist plot (Fig. 8) shows a small semicircle in the high-frequency region and a nearly straight line in the low-frequency region. The high-frequency semicircle represents the charge-transfer resistance at the electrode-electrolyte interface, while the linear part at low frequency corresponds to ion diffusion and capacitive behaviour.

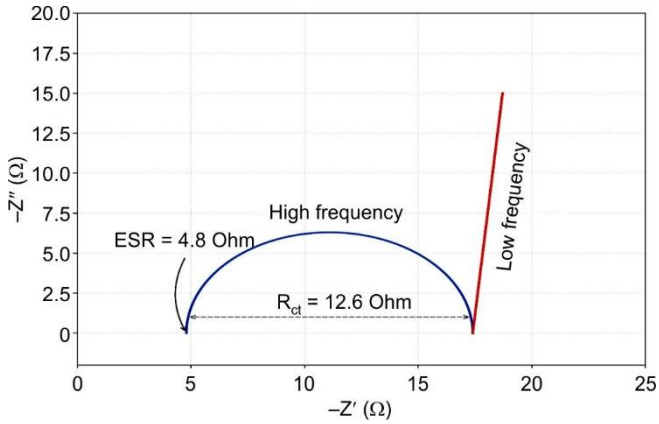

Fig. 8. EIS Nyquist plot of the solid-state supercapacitor showing ESR and charge transfer resistance (R_{ct})

From equivalent circuit fitting, an equivalent series resistance (ESR) of 4.8 Ω and a charge-transfer resistance (R_{ct}) of 12.6 Ω were obtained. The low ESR value indicates good electrical contact between the current collector and $CsSnI_3$ electrode, along with high electronic conductivity of $CsSnI_3$ and efficient Na^+ ion transport through the PNPS3 gel polymer electrolyte. The relatively low R_{ct} value suggests fast interfacial charge-transfer kinetics, which can be attributed to the layered ion-transport pathways provided by 2D BA_2SnI_4 nanosheets, uniform polymer structure and improved dielectric properties of the composite electrolyte.

Furthermore, the nearly vertical line in the low-frequency region indicates rapid ion diffusion and low polarization, confirming excellent capacitive behaviour with the minimal diffusion resistance. Compared to pure PVDF-HFP electrolyte systems, the PNPS3-based device shows about 38% lower R_{ct}, demonstrating the synergistic interaction between conductive $CsSnI_3$ electrodes and the BA_2SnI_4-reinforced polymer electrolyte. This confirms the effectiveness of the optimized composite design for the high-performance solid-state supercapacitors.

Cycling stability: The long-term cycling stability of the optimized symmetric solid-state supercapacitor was measured by continuous GCD testing at 2 A g^{-1} for 5000 cycles. The device initially produces a specific capacitance of 167 F g^{-1}, which slightly decreased to 154 F g^{-1} after 5000 cycles, corresponding to a high capacitance retention of 92% (Fig. 9). The coulombic efficiency remained above 97% throughout the cycling, indicating highly reversible charge-discharge behaviour with minimal energy loss. This excellent stability can be attributed to the structural stability of black orthorhombic $CsSnI_3$ phase, suppression of Sn^{2+} oxidation within the PNPS3 electrolyte, strong electrode–electrolyte interfacial adhesion, and the good mechanical strength of the PNPS3 membrane, which remains stable even after repeated bending cycles.

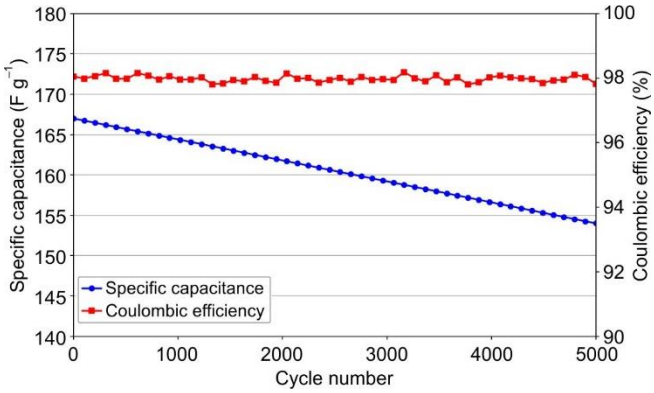

Fig. 9. Cycling stability and coulombic efficiency of the solid-state supercapacitor over 5000 charge-discharge cycles

Conclusion

In this work, a solid-state symmetric supercapacitor was developed using lead-free $CsSnI_3$ perovskite electrodes and a 2D Ruddlesden-Popper BA_2SnI_4-reinforced PVDF-HFP/$NaPF_6$ gel polymer electrolyte. The combined design of optimized electrodes and nano-structured electrolyte improved ionic conductivity, interfacial stability, mechanical strength and the electrochemical performance. The optimized PNPS3 electrolyte with 15 wt.% BA_2SnI_4 showed the highest ionic conductivity (1.12 mS cm^{-1}) and lowest bulk resistance (92 Ω), due to effective ion-transport pathways formed by uniformly dispersed 2D nanosheets. The structural analysis confirmed the phase-pure, highly crystalline orthorhombic black $CsSnI_3$, ensuring good electronic conductivity. The FESEM and TGA results indicated uniform morphology and improved thermal stability (degradation onset at 292 ºC), confirming strong polymer-filler interaction. The symmetric $CsSnI_3$/PNPS3/$CsSnI_3$ device delivered a specific capacitance of 186 F g^{-1} at 1 A F g^{-1}, low IR drop (0.042 V), low R_{ct} (12.6 Ω), energy density of 25.8 Wh kg^{-1} and power density of ~500 W kg^{-1}. It retained 92% capacitance after 5000 cycles with >97% coulombic efficiency. The electrolyte membrane also remained stable after more than 1000 bending cycles, demonstrating good flexibility. Based on these results, the synergistic interaction between black-phase $CsSnI_3$ electrodes and the BA_2SnI_4-

reinforced gel polymer electrolyte confirmed the enhancement of the ion transport, reduced degradation and improved interfacial contact, making this system promising for flexible and portable solid-state energy storage applications.

CONFLICT OF INTEREST

The authors declare that there is no conflict of interests regarding the publication of this article.

DECLARATION OF AI-ASSISTED TECHNOLOGIES

During the preparation of this manuscript, the authors used an AI-assisted tool(s) to improve the language. The authors reviewed and edited the content and take full responsibility for the published work.

REFERENCES

1. Y. Qian, Q. Ruan, M. Xue and L. Chen, *J. Energy Chem.*, **89**, 41 (2024); https://doi.org/10.1016/j.jechem.2023.10.028
2. M. Neelakandan, P. Dhandapani, S. Ramasamy, R. Duraisamy, S.J. Lee and S. Angaiah, *RSC Adv.*, **15**, 16766 (2025); https://doi.org/10.1039/D5RA01950H
3. V. Viswanathan, J. Yesuraj, M. Ramesh, K. Kim and K. Biswas, *J. Energy Storage*, **78**, 109968 (2024); https://doi.org/10.1016/j.est.2023.109968
4. N.K. Noel, S.D. Stranks, A. Abate, C. Wehrenfennig, S. Guarnera, A.A. Haghighirad, A. Sadhanala, G.E. Eperon, S.K. Pathak, M.B. Johnston, A. Petrozza, L.M. Herz and H.J. Snaith, *Energy Environ. Sci.*, **7**, 3061 (2014); https://doi.org/10.1039/C4EE01076K
5. B.K. Ravidas, M.K. Roy and D.P. Samajdar, *Solar Energy*, **249**, 163 (2023); https://doi.org/10.1016/j.solener.2022.11.025
6. Z. Gao, H. Zhou, K. Dong, C. Wang, J. Wei, Z. Li, J. Li, Y. Liu, J. Zhao and G. Fang, *Nano-Micro Lett.*, **14**, 215 (2022); https://doi.org/10.1007/s40820-022-00964-9
7. I. Benaicha, S. Amraoui, J. Mhalla, Y. Ait-Alla, H. Diyagh, M. Simassa, K. Nouneh, A. Fahmi, M. Fahoume and A. Qachaou, *Results Eng.*, **27**, 106845 (2025); https://doi.org/10.1016/j.rineng.2025.106845
8. H. Wang, B. Zhao, W. Tan and H. Wang, *J. Mater. Sci. Mater. Electron.*, **36**, 1394 (2025); https://doi.org/10.1007/s10854-025-15480-w
9. A. Ivanova, M. Golikova, L. Luchnikov, P. Gostishchev, I. Shetinin, V. Voronov, D. Saranin and V. Khovaylo, *Clean Energy*, **8**, 109 (2024); https://doi.org/10.1093/ce/zkae028
10. S. Ahmed, A. Majid, M. Nasir, G.U. Islam, S.A. Ullah, N. Maqbool, A. Noreen, H. Kiran, M. Ali, T. Saidani and M.I. Khan, *J. Inorg. Organomet. Polym. Mater.*, **35**, 6208 (2025); https://doi.org/10.1007/s10904-025-03649-z
11. X. Dong, X. Li, X. Wang, Y. Zhao, W. Song, F. Wang, S. Xu, Z. Miao and Z. Wu, *Adv. Mater.*, **36**, e2313056 (2024); https://doi.org/10.1002/adma.202313056
12. J.F. Dalmedico, D.N. Silveira, C.M.O. Bastos, C.R. C Rêgo, A. Cavalheiro Dias, D. Guedes-Sobrinho and M.J. Piotrowski, *J. Phys. Chem. C*, **129**, 9646 (2025); https://doi.org/10.1021/acs.jpcc.5c01707
13. J. Wang, H. Shen, W. Li, S. Wang, J. Li and D. Li, *Adv. Sci.*, **6**, 1802019 (2019); https://doi.org/10.1002/advs.201802019
14. P. Darman, A. Yaghoobi and S. Darbari, *Sci. Rep.*, **13**, 8374 (2023); https://doi.org/10.1038/s41598-023-35546-1
15. X. Han, Y. Zheng, S. Chai, S. Chen and J. Xu, *Nanophotonics*, **9**, 1787 (2020); https://doi.org/10.1515/nanoph-2020-0038
16. K. Luo, L. Yi, X. Chen, L. Yang, C. Zou, X. Tao, H. Li, T. Wu and X. Wang, *J. Electroanal. Chem.*, **895**, 115462 (2021); https://doi.org/10.1016/j.jelechem.2021.115462
17. J. Zhang, B. Sun, X. Huang, S. Chen and G. Wang, *Sci. Rep.*, **4**, 6007 (2014); https://doi.org/10.1038/srep06007
18. D. Mouraliraman, N. Shaji, S. Praveen, M. Nanthagopal, C.W. Ho, M. Varun Karthik, T. Kim and C.W. Lee, *Nanomaterials*, **12**, 1056 (2022); https://doi.org/10.3390/nano12071056
19. P. Shabeeba, J. kavil, P. Shameela, P. Sreya and N. Aparna, *Next Materials*, **6**, 100330 (2025); https://doi.org/10.1016/j.nxmate.2024.100330
20. I.R. Varma, V.R. Jeedi, K.K. Ganta, R. Katuri, N. Kundana, G. Upender, C.V.K. Reddy, V. Suryanarayana and S. Ramesh, *J. Polym. Res.*, **32**, 166 (2025); https://doi.org/10.1007/s10965-025-04399-9
21. X. Sun and H. Liu, *J. Polym. Res.*, **31**, 53 (2024); https://doi.org/10.1007/s10965-024-03907-7
22. G. Behzadi Pour, H. Nazarpour Fard and L. Fekri Aval, *Gels*, **10**, 803 (2024); https://doi.org/10.3390/gels10120803
23. J. Jie, Y. Liu, L. Cong, B. Zhang, W. Lu, X. Zhang, J. Liu, H. Xie and L. Sun, *J. Energy Chem.*, **49**, 80 (2020); https://doi.org/10.1016/j.jechem.2020.01.019
24. H. Fan, C. Yang, X. Wang, L. Liu, Z. Wu, J. Luo and R. Liu, *J. Electroanal. Chem.*, **871**, 114308 (2020); https://doi.org/10.1016/j.jelechem.2020.114308
25. U.Y. Bello, P.S. Dhapola, H. Ahuja and P.K. Singh, *Mater. Today Proc.*, **49**, 3449 (2022); https://doi.org/10.1016/j.matpr.2021.03.498
26. Z.T. Huang, J.Y. Lin and M. Krajewski, *Electrochim. Acta*, **526**, 146192 (2025); https://doi.org/10.1016/j.electacta.2025.146192
27. X. Yao, L. Lan, Q. Hun, X. Lu, J. Wei, X. Liang, P. Shen, Y. Long and Y. Guo, *Gels*, **11**, 317 (2025); https://doi.org/10.3390/gels11050317
28. R. Huang, R. Xu, J. Zhang, J. Wang, T. Zhou, M. Liu and X. Wang, *Nano Res.*, **16**, 9480 (2023); https://doi.org/10.1007/s12274-023-5707-x
29. D. Deb, Flexible Polymerized Ionic Liquids Gel Polymer Electrolytes for Supercapacitor Application, In: Ionic Liquids-Recent Advance, IntechOpen, p. 89 (2024).
30. A.D. Shuaibu, S.S. Shah, A.S. Alzahrani and M.A. Aziz, *J. Energy Storage*, **107**, 114851 (2025); https://doi.org/10.1016/j.est.2024.114851